Iron(VI) in Tetrahedral Oxo Coordination: A Single Crystal EPR Study

B. Wagner,[†] D. Reinen,*[,†] Th. C. Brunold,[‡] and H. U. Güdel[‡]

Fachbereich Chemie and Zentrum für Materialwissenschaften der Philipps-Universität, Hans-Meerwein-Strasse, D-35043 Marburg, Germany, and Institut für anorganische und physikalische Chemie, Freiestrasse 3, Universität Bern, CH-3000 Bern 9, Switzerland

Received August 10, 1994[⊗]

The single crystal and powder EPR spectra of Fe(VI) in the host structures K_2MO_4 (M = Cr, S, Se) were analyzed with respect to the fine structure parameters D and E. In the case of K_2SeO_4, which possesses three structural modifications in dependence on temperature, the number of crystallographically inequivalent Fe(VI) positions and the changes of the extent of polyhedral distortion could be followed by passing the two phase transitions. AOM calculations were used in order to assign the various EPR signals to the different sites.

Introduction

Fe(VI)-doped K_2MO_4 (M = S, Cr, Se) single crystals exhibit interesting luminescence properties, involving the excited tetrahedral $_a{}^1E$ state of the d^2 configurated Fe(VI) center in tetraoxo coordination.[1,2] From the optical spectra[2] a Δ parameter of $\simeq$13 000 cm^{-1} and a strongly reduced nephelauxetic ratio $\beta = B/B_0 \simeq 0.29$ is derived [free ion values: $B_0 = 1300$ cm^{-1}, $C_0/B_0 = 4.2_5$, $\zeta = 670$ cm^{-1} [3]]. The β ratio seems to reflect not only the expected trend for the series Cr(IV) (0.47),[4] Mn(V) (0.37),[5,6] and Fe(VI) but also the rather pronounced instability of the (+VI) oxidation state for iron (see below). This is confirmed[2] by the appearance of the first ligand-to-metal charge transfer band at $\simeq$19 000 cm^{-1}, in comparison to 24 000 cm^{-1} for the MnO_4^{2-} polyhedron in alkaline solution.[5]

In order to obtain further insight into the properties of the Fe−O bond and the site geometry of the FeO_4 polyhedra in the various host lattices via the fine structure tensor we have performed EPR single crystal and powder investigations. So far zero field splitting parameters and g values are reported only for Fe(VI)-doped K_2CrO_4 in single crystal[7,8] and powder investigations.[8] The reported values are

$$D = 0.10_8\ cm^{-1} \quad E = 0.01_7\ cm^{-1} \quad g = 1.99_6 \quad (77\ K)$$

with very small angular contributions to the **g** tensor and a tiny anisotropy. The effective spin−orbit (LS) coupling constant, as deduced from eq 1 with $\Delta \simeq 13\,000$ cm^{-1} would be only about 20 cm^{-1}. This extremely low value will be commented upon below.

$$g = g_0 - 4\zeta_{eff}/\Delta \qquad (1)$$

The chosen host lattices K_2CrO_4, β-K_2SO_4, and K_2SeO_4 crystallize at room temperature in the orthorhombic space group *Pnam* (No. 62) with $Z = 4$. The spacings and bond angles of the MO_4 polyhedra of the host compounds are collected in Table 1.

Table 1. Bond Lengths, O(i)−M−O(j) Bond Angles (deg), and Symmetry Parameter δ (deg)[a] of the MO_4 tetrahedra in K_2MO_4 [M: S,[9,10] Cr,[11] Se;[12] 298 K][b] and Unit Cell Dimensions (Å)

M	M−O	$i = 1, j = 1'$	1,2 (2x)	1,3 (2x)	2,3	δ
S[9]	1.50	109.8	109.3	109.5	109.6	0.1_5
Cr	1.60_5	110.6	109.4	109.1	109.2	0.4
Se	1.65(1)	110.5(4)	108.4(3)	109.8(4)	109.8(6)	0.7

M	a	b	c
S[10]	7.456	10.08	5.776
Cr	7.61	10.40	5.92
Se	7.661	10.466	6.003

[a] $\delta = {}^1/_6 \sum_{i=1}^{6} |2\theta_i - 2\theta_t|$; $2\theta_t$ is the tetrahedral angle. [b] The published data in refs 9−11 are of rather low precision.

1. The MO_4 point symmetry is C_s with two magnetically inequivalent polyhedra in the unit cell. The deviation of the MO_4 geometry from T_d symmetry is small in all cases. The M, O(2), and O(3) atoms lie in the (001) plane of the lattice, the latter being the mirror plane of the tetrahedron with respect to the two O(1) atoms (Figure 1). While these conditions are given by symmetry, the special positions of M and O(3) are such that the M−O(3) bond direction is oriented parallel to a within a few degrees.

The MO_4 tetrahedra in the compounds K_2MO_4 (M = S, Cr, Se) are slightly deformed with O−M−O angles varying between 109 and 110.5° (Table 1). The three nearly equal O(3)−M−O(1,1′,2) angles suggest a pseudo C_{3v} symetry, but the nonequivalence of the O(1)−M−O(1′) and O(2)−M−O(1,1′) angles indicates a very distinct superimposed lower-symmetry distortion component. Alternatively one may assume an approximate C_{2v} symmetry with the pseudo C_2 axis bisecting the O(1)−M−O(1′) angle. However, the differing O(2)−M−O(1,1′) and O(3)−M−O(1,1′) angles reduce the symmetry again to C_s. After all it is expected by the given symmetry arguments that the g and fine structure components, derived from the angular dependence of the EPR spectra, have orientations as follows. Two components should be found in the (001) crystal planes (Figure 1), with one of them near the M−O(3) bond (pseudo C_3 axis) or shifted toward the pseudo C_2 axis. The third component is expected to have an orientation perpendicular to the C_s molecular plane ((001) crystal plane).

Experimental Section

Single crystals of Fe(IV)-doped K_2MO_4 salts (M = S, Cr, Se) were synthesized according to preparation methods reported elsewhere.[1,2]

[†] Philipps-Universität.
[‡] Universität Bern.
[⊗] Abstract published in *Advance ACS Abstracts,* March 1, 1995.

(1) Herren, M.; Güdel, H. U. *Inorg. Chem.* **1992**, *18*, 3683.
(2) Brunold, Th. C.; Hauser, A.; Güdel, H. U. *J. Lumin.* **1994**, *59*, 321.
(3) Warner, B.; Kirkpatrick, R. C. *Mon. Not. R. Astr. Soc.* **1969**, *144*, 397.
(4) Kesper, U.; Atanasov, M.; Roos, J.; Reinen, D. *Inorg. Chem.* **1995**, *34*, 184.
(5) Lachwa, H.; Reinen, D. *Inorg. Chem.* **1989**, *28*, 1044.
(6) Atanasov, M.; Adamsky, H.; Reinen, D. Submitted for publication in *J. Chem. Phys.*
(7) Carrington, A.; Ingram, D. J. E.; Lott, K. A. K.; Schonland, D.; Symons, M. C. R. *Proc. R. Soc. Lett.* **1960**, *A254*, 101.
(8) Debuyst, R.; Dejehet, F.; Apers, D. *J. Inorg. Nucl. Chem.* **1975**, *37*, 338.
(9) *Strukturber.* **1937**, *2*, 86−88.
(10) Robinson, M. T. *J. Phys. Chem.* **1958**, *62*, 925.
(11) Zachariasen, W. H.; Ziegler, G. E. *Z. Kristallogr.* **1931**, *80*, 164.
(12) Kalman, A.; Stephens, J. S.; Cruickshank, D. W. J. *Acta Crystallogr.* **1970**, *B26*, 1451.

0020-1669/95/1334-1934$09.00/0

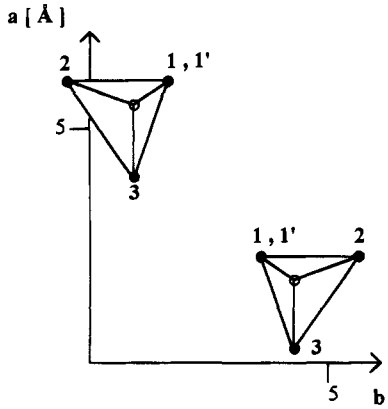

Figure 1. Projection of the two magnetically inequivalent MO_4 polyhedra in the structures of K_2MO_4 (M = S, Cr, Se) into the (001) plane ($z = {}^1/_4$). The given geometric relations are those for K_2SO_4, with the O(1) and O(1′) atoms having positions at $\delta z = \pm 0.22$ (± 1.27 Å) with respect to this plane.

The EPR spectra at X and Q band frequencies and between 4 and 298 K were taken with a Bruker spectrometer (ESP 300 E). The crystals, which usually were of a distorted cuboctahedral shape, were adjusted in the magnetic field assuming that the crystal axes equal the crystallographic axes in the reciprocal lattice.

Results and Discussion

d^2 configurated cations possess a $^3A_2$ ground state in T_d ligand fields and undergo zero-field splitting effects, if tetrahedron distortions are present. The EPR spectra of spin-triplet states are described by the spin Hamiltonian of eq 2 if a coordinate

$$H = \beta \hat{H} \hat{\hat{g}} \hat{S} + \hat{S} \hat{\hat{D}} \hat{S} \tag{2}$$

$$\hat{S} \hat{\hat{D}} \hat{S} = D(S_z^2 - {}^1/_3 S(S+1)) + E(S_x^2 - S_y^2)$$

system is chosen, where the zero-field-splitting tensor **D** is diagonal. The D_x, D_y, and D_z components of **D** are related to the commonly used zero-field-splitting parameters D and E by eq 3. The six possible $\Delta M_s = 1$ transitions in a magnetic field

$$D = {}^1/_2(2D_z - D_x - D_y) \qquad E = {}^1/_2(D_x - D_y) \tag{3}$$

$$D_x + D_y + D_z = 0$$

induced by an orthorhombic zero-field splitting together with those corresponding to $\Delta M_s = 2$ are given in eq 4.[13]

$$\begin{aligned}
a^2 H_{x1(2)}{}^2 &= (H_0 \mp D' \pm E')(H_0 \pm 2E') \\
a^2 H_{y1(2)}{}^2 &= (H_0 \mp D' \mp E')(H_0 \mp 2E') \\
a^2 H_{z1(2)}{}^2 &= (H_0 \mp D')^2 - E'^2 \\
a^2 H_{x3(3)}{}^2 &= {}^1/_4(H_0^2 - (D' + E')^2) \\
a^2 H_{z3}{}^2 &= {}^1/_4(H_0^2 - 4E'^2)
\end{aligned} \tag{4}$$

In powder spectra the latter three transitions are not observed, but the signals H_{min} and H_{dq} appear—both also connected with $\Delta M_s = 2$.[13] H_{min} characterizes the low-field limit of the spectrum, while H_{dq} corresponds to a double-quantum absorption (eq 5). H_0 is defined by $h\nu = g_0 \beta H_0$ (ν is the microwave

$$a^2 H_{min}{}^2 = {}^1/_4(H_0^2 - {}^4/_3(D'^2 + 3E'^2)) \tag{5}$$

$$a^2 H_{dq}{}^2 = H_0^2 - {}^1/_3 D'^2 - E'^2$$

frequency and β the Bohr magneton), and the coefficient a is the ratio g/g_0. The zero-field-splitting parameters $D(E)$ in wavenumbers are related to $D'(E')$ by $D(E) = D'(E')\nu/cH_0$. The **g** tensor was regarded as isotropic because the orbital contributions are very small (eq 1) .

Fe(VI)-Doped K_2CrO_4. The angular dependence of the EPR signals of Fe(VI)-doped K_2CrO_4 at 120 K is shown in Figure 2. In the (001) plane two positions are clearly resolved, with the highest and lowest field transitions (H_{y1} and H_{y2}, respectively—eq 4) appearing in directions, which deviate by about $\pm 15°$ from the M−O(3) bond vector in accord with the presence of two magnetically inequivalent sites. Apparently the D_y tensor components orient themselves very near to the pseudo C_3 axes of the two CrO_4^{2-} tetrahedra (approximate C_{3v} symmetry, Figure 1). In the (010) and (100) planes the $H_{z1(2)}$ transitions are seen parallel to the c axis. Along a and b, however, the projections of $H_{y1(2)}$ and $H_{x1(2)}$ on those directions should be observed, which are identical for polyhedra I and II. Assuming a canting angle of 18° the maximum and minimum magnetic fields along a and b can indeed be reproduced from H_y and H_x—in excellent agreement with the angle derived from the angular dependence in the (001) plane (Figure 2). The calculated zero-field-splitting parameters ($g = 1.99_6$) $D = 0.10_3$ cm^{-1} and $E = 0.01_4$ cm^{-1} (120 K) nicely match with those reported in the literature.[7,8] Slightly higher values result from our low-temperature powder spectra [$D = 0.11_2$ cm^{-1}, $E = 0.02_0$ cm^{-1} (10 K)]. We may conclude, that the D tensor components (eq 3) are correlated with the FeO_4 polyhedron geometry such that $|D_z|$ (0.07_5 cm^{-1}, 10 K) has an orientation parallel to the crystallographic c axis, while $|D_y|$ (0.05_8 cm^{-1}, 10 K) deviates from the M−O(3) bond direction by an angle of 15° ± 3°, in reasonable agreement with reported results for 77 K (11°).[7,8] $|D_x|$ (0.01_7 cm^{-1}, 10 K) is located in the (001) plane perpendicular to D_y. The D and E values derived from the single crystal data at 295 K are $\simeq 0.07_5$ cm^{-1} and $\approx 0.00_5$ cm^{-1}, respectively, and hence significantly smaller than those obtained at lower temperatures—indicating less distinct site distortions. The nearly vanishing orthorhombic parameter indicates an almost perfect C_{3v} site symmetry, which is in contrast to the available, not very precise, structural data for the CrO_4^{2-} host polyhedron (Table 1) but supported by the angular dependence in the (001) plane (Figure 3). The deviation of $|D_y|$ ($\simeq 0.03$ cm^{-1}) from the M−O(3) bond direction is so small that the two positions cannot be resolved in the EPR spectra within the line width anymore. Apparently the extent of the site distortion and the angle between the D_y tensor component and the M−O(3) bond direction (Figure 1) increase with decreasing temperature.

Fe(VI)-Doped β-K_2SO_4. The angular dependence of the EPR signals for Fe(VI)-doped β-K_2SO_4 in three mutually perpendicular planes at 110 K (Figure 4) is completely different compared with the one in Figure 2 and indicative for the—in very good approximation verified—condition $D = 3E$, leading to the $\Delta M_s = \pm 1, \pm 2$ transitions in eq 6

$$\begin{aligned}
a^2 H_{x1}{}^2 &= a^2 H_{x2}{}^2 &&\simeq H_0^2 - 4E'^2 \\
a^2 H_{y1(2)}{}^2 &= a^2 H_{z1(2)}{}^2 &&\simeq (H_0 \mp 3E')^2 - E'^2 \\
a^2 H_{x3}{}^2 & &&\simeq {}^1/_4(H_0^2 - 16E'^2) \\
a^2 H_{y3}{}^2 &= a^2 H_{z3}{}^2 &&= {}^1/_4(H_0^2 - 4E'^2)
\end{aligned} \tag{6}$$

derived from eq 4 and to $D_x = 0$ and $-|D_y| = |D_z| = 2E$ (see eq 3). H_{min} and H_{dq} are expected to collapse with H_{x3} and $H_{x1,2}$, respectively. Indeed the EPR powder spectrum is in full accord

(13) Wasserman, E.; Snyder, L. C.; Yager, W. A. *J. Chem. Phys.* **1964**, *41*, 1763.

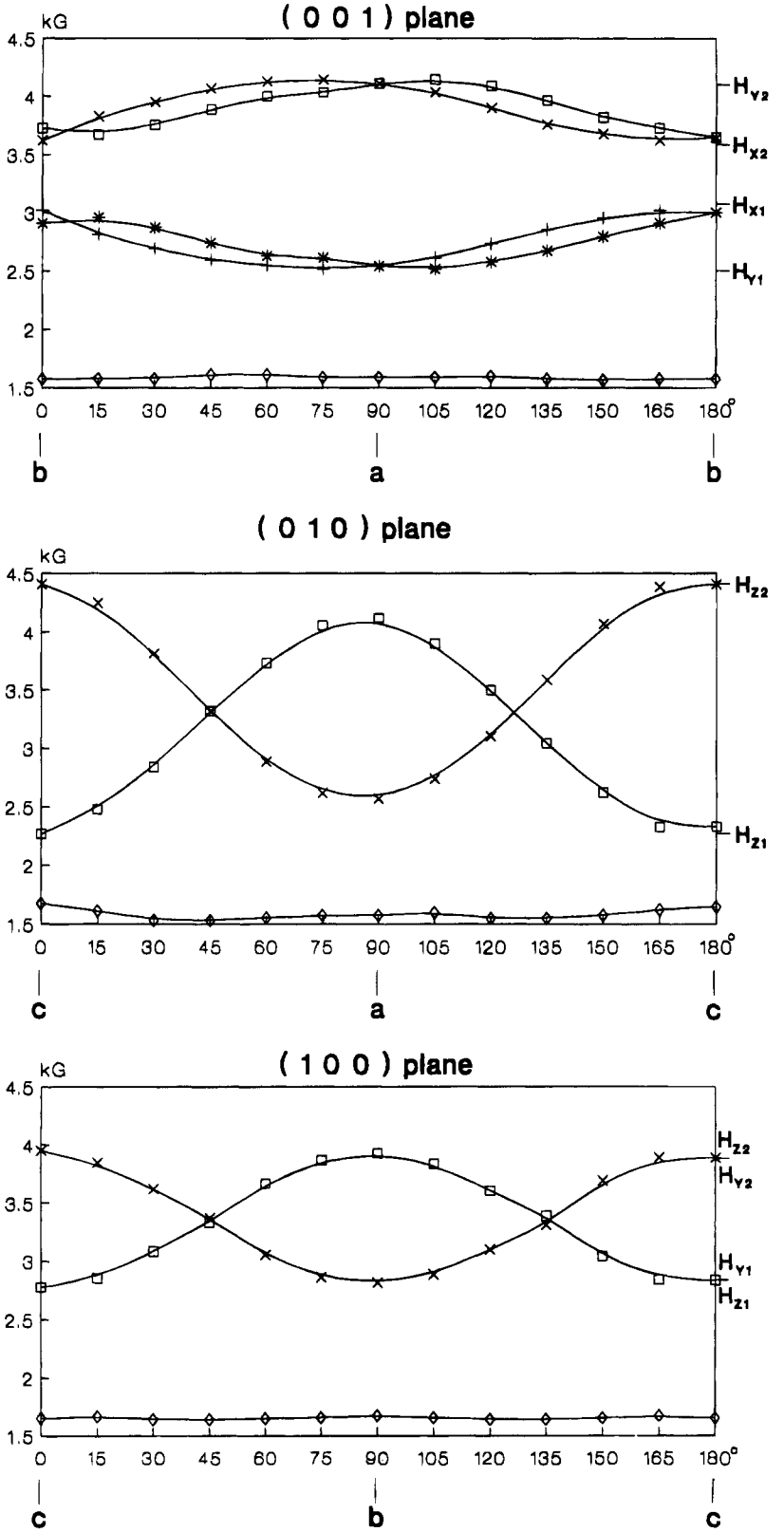

Figure 2. Angular dependence of the EPR signals (X band) of Fe(VI)-doped K_2CrO_4 (3 mol %) at 120 K in three mutually perpendicular planes. (The slight irregularities in the (001) plane are due to a small crystal misalignment of about 5°. The expected splitting of the $\Delta M_s = \pm 2$ transitions into two is not resolved.)

with this assumption, exhibiting besides the H_{min} transition central nearly coinciding $H_{x1,2}$ and H_{dq} signals, which are symmetrically flanked by the two $H_{z1(2)} = H_{y1(2)}$ transitions. From the angular dependence in the (001) plane we may conclude that the D tensor components possess (nearly) identical orientations for the two sites, with $|D_x|$ and $|D_y|$ ($=|D_z|$) having orientations parallel to a and b, respectively. Actually two signals are resolved in each H_i (i = 1, 2) transition at certain angles, however, indicating that two sites with tiny deviations of $D_{x1(2)}$ and $D_{y1(2)}$ from a and b indeed exist. The D_y components, which were associated with directions near the M−O(3) bond in the case of Fe(IV)-doped K_2CrO_4, have moved to an orientation nearly parallel to b (see Introduction), forming an angle of ≈35° with the pseudo C_2 axis (Figure 1). The D (≃3E) parameter calculated from the EPR powder spectra between 130 and 4 K at X and Q band conditions (g = 1.99$_6$)

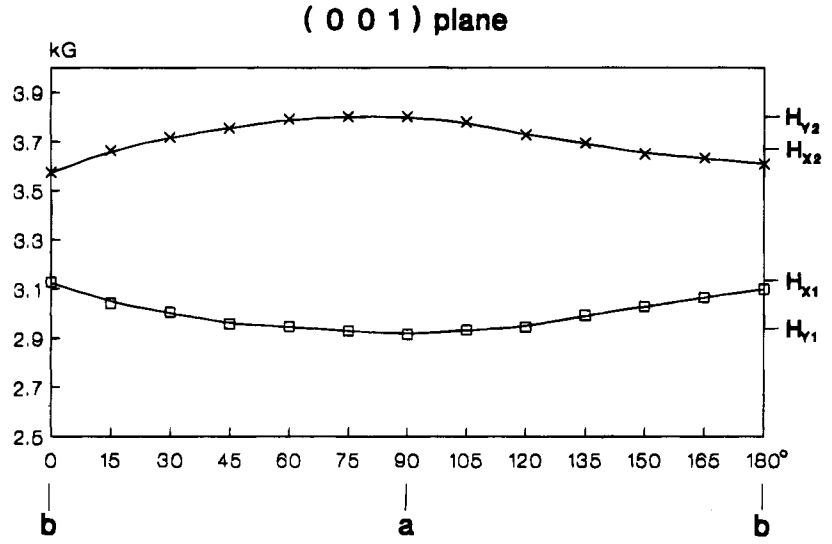

Figure 3. Angular dependence of the EPR signals (X band) of Fe(VI)-doped K_2CrO_4 (3 mol %) at 295 K in the (001) plane. (The signals are rather broad implying an experimental error of about ±40 G.)

is 0.05_8 cm^{-1} ($D_x \simeq 0$, $-|D_y| = |D_z| = 0.03_8$ cm^{-1}) and perfectly agrees with the values obtained from the single crystal spectra at 110 and 4 K. The small D value is in accord with the rather tiny deviations of the bond angles within the SO_4^{2-} tetrahedra from 109.5° (Table 1).

Fe(VI)-Doped K_2SeO_4. K_2SeO_4, which crystallizes in the space group *Pnam* at 298 K [12] as β-K_2SO_4 and K_2CrO_4 (Table 1), undergoes phase transitions at T_i = 130 K and T_c = 93 K, the low-temperature phase L being characterized by an enlarged unit cell with $a' = 3a$.[14] The latter modification is ferroelectric, possessing the noncentrosymmetric space group $Pna2_1$.[15] The SeO_4^{2-} tetrahedra are rotated with respect to those in the *Pnam* structure (Figure 1) by 12 different sets of angles around the *a*, *b*, and *c* axes.[16] From these 12 magnetically inequivalent polyhedra three are crystallographically independent and possess rather different and considerable distortions.[16] The intermediate phase I is incommensurate and is described on the basis of a modulated *Pnma* space group.[17]

The angular dependence of the EPR signals for the high-temperature phase H is shown in Figure 5. As in the previous case of Fe(VI) in β-K_2SO_4 the condition $D = 3E$ is approximately obeyed [$D = 0.09_0$ cm^{-1}; $E = 0.02_8$ cm^{-1}; $g = 1.99_6$ (140 K)]. In contrast to Figure 4, however, two magnetically inequivalent polyhedra are clearly distinguished in the (001) plane, with the D_y component oriented nearly parallel to the pseudo-C_2 axis. Comparing the D_y orientation in the three investigated compounds with respect to the Fe−O(3) bond direction (||*a*, pseudo-C_3 axis), we find a deviation of ≃15° for the K_2CrO_4 ($D \gg E$), ≃52.5° for H-K_2SeO_4 ($D > 3E$), and ≃90° ($D = 3E$) for the β-K_2SO_4 host structure. It is expected that the average deviation of the O(i)−M−O(j) bond angles from the ideal tetrahedral angle δ (Table 1) should reflect the total spread of the zero-field-splitting $D + E$. Due to the rather low precision of the crystallographic data this is only very roughly the case, however, with $D + E$ being ≈0.08, ≈0.11, and ≈0.11 cm^{-1} at 130 K for Fe(VI)-doped β-K_2SO_4, K_2CrO_4, and K_2SeO_4, respectively. Nearly the same zero-field-splitting parameters as those derived from the single crystal data are calculated from the X-band and Q-band powder spectra of Fe(VI) in K_2SeO_4 at 140 K (Figure 6).

The presence of 12 magnetically inequivalent sites in the L phase leads to EPR single crystal spectra at 5 K showing a large number of signals in the region of the ($\Delta M_s = \pm 1$) transitions, which we were able to analyze only for a few magnetic field directions. The EPR spectra of the incommensurate I phase are similarly complex. The positional parameters in the space group $Pna2_1$ of the L phase are such that each group of four symmetry-related polyhedra has identical projections along the crystallographic [001] axis. Accordingly only the three crystallographically independent sites should be seen in this direction in the EPR spectra at low temperatures, in perfect agreement with the experimental evidence (Figure 7).

Very informative with respect to the phase transitions and the number of Fe(VI) sites is the temperature dependence of the EPR spectra. The powder spectra are expected to reflect only positions with different extents of distortion *separately*, because groups of polyhedra, which are distinguished merely by different orientations of the molecular *g* tensor, yield the same spectrum. This is indeed nicely demonstrated for X-band frequencies in Figures 8 and 9. The H_{min} signal of the H-phase is split into two at ≲120 K in the I-phase region, roughly 10 K below the critical temperature of the H → I transition, indicating the presence of two crystallographically independent sites. This finding is somewhat unexpected regarding the available crystallographic data.[17] In the L phase below 90 K three different sites appear, in accord with the structure determination.[16] The low-temperature spectra (Figure 8) are dominated in intensity by the three H_{min} transitions. This behavior is expected at X band frequencies for D values around 0.2 cm^{-1} and strong orthorhombic symmetry components (see the powder spectra simulations in ref 18). Table 2 lists zero-field-splitting parameters calculated from H_{min} with the limiting assumptions $D = 3E$ and $E = 0$, respectively, for some selected temperatures.

From the temperature dependence of the single crystal spectra along the *c* axis (Figure 7) essentially the same information as that from Figure 9 can be deduced. The behavior of the ($\Delta M_s = \pm 2$) transitions follows the one of H_{min}, though their intensity is much smaller and the signals frequently disappear in the background noise. The ($\Delta M_s = \pm 1$) transitions behave rather differently with a slight decrease of the separation to H_0 when lowering the temperature—in contrast to the expected increase due to larger zero-field splittings at low temperatures. We can explain this experimental finding as follows. Because the local symmetry plane of the SeO_4 host tetrahedra vanishes at 90 K (I → L phase transition), the D_z fine structure component may

(14) Ohama, N. *Mater. Res. Bull.* **1974**, *9*, 283.
(15) Iizumi, M.; Axe, J. D.; Shirane, G. *Phys. Rev.* **1977**, *B15*, 4392.
(16) Yamada, N.; Ono, Y.; Ikeda, T. *J. Phys. Soc. Jpn.* **1984**, *53*, 2565.
(17) Yamada, N.; Ikeda, T. *J. Phys. Soc. Jpn.* **1984**, *53*, 2555.
(18) Mabbs, F. E.; Collison, D. *EPR of d Transition Metal Compounds*; Elsevier: Amsterdam, 1992.

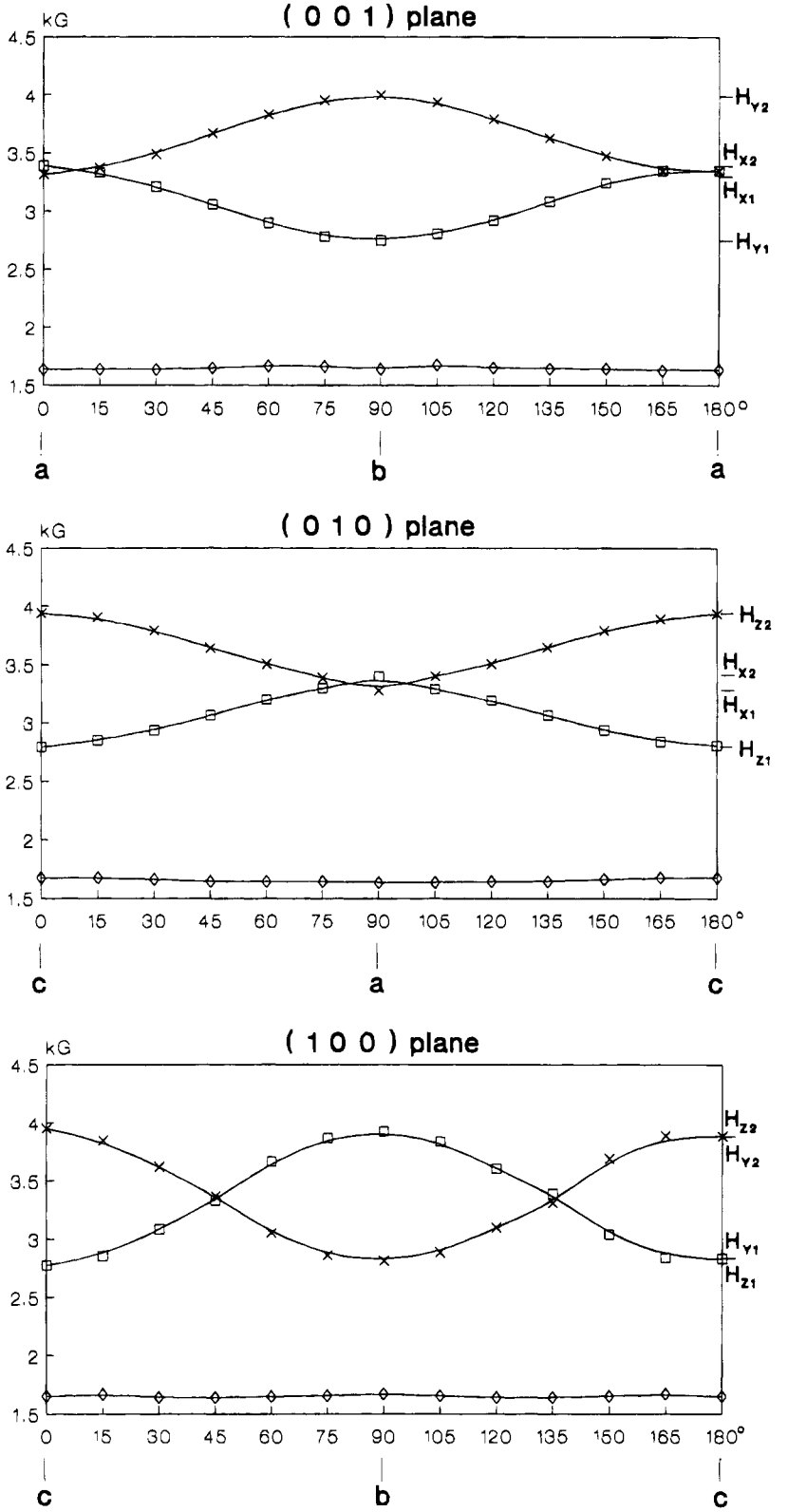

Figure 4. Angular dependence of the EPR signals (X band) of Fe(VI)-doped β-K_2SO_4 (0.2 mol %) at 110 K in three mutually perpendicular planes. (In certain directions in the (001) plane two signals are resolved, the averaged value being given in the figure.)

not correlate with the [001] direction anymore. With the assumption that a rotation of D_x toward the c axis occurs, it is possible to understand the temperature dependence. With inspection of eq 6, it is easily deduced that the transition from $H_{z1(2)}$ to $H_{x1(2)}$ diminishes drastically the separation to H_0, while the reverse effect is expected when switching from H_{z3} to H_{x3}. Apparently the increase of D ($\simeq 3E$) when passing from $T >$ 130 K to the three sites at very low temperatures nearly compensates the described field shift in the first case whereas it becomes even larger for the ($\Delta M_s = \pm 2$) transitions. Numeric estimations confirm the concept of a rotation of the g tensor components in the described sense below 90 K.

We may compare the EPR results with those from luminescence spectroscopy, analyzing the tetrahedral $^1E \rightarrow {}^3A_2$ transition (Table 3). Three differently distorted sites are distinguished in the low-temperature phase but—in contrast to the EPR evidence—in the I phase as well.[2] Though both techniques, EPR and luminescence spectroscopy, reflect geometrical deviations

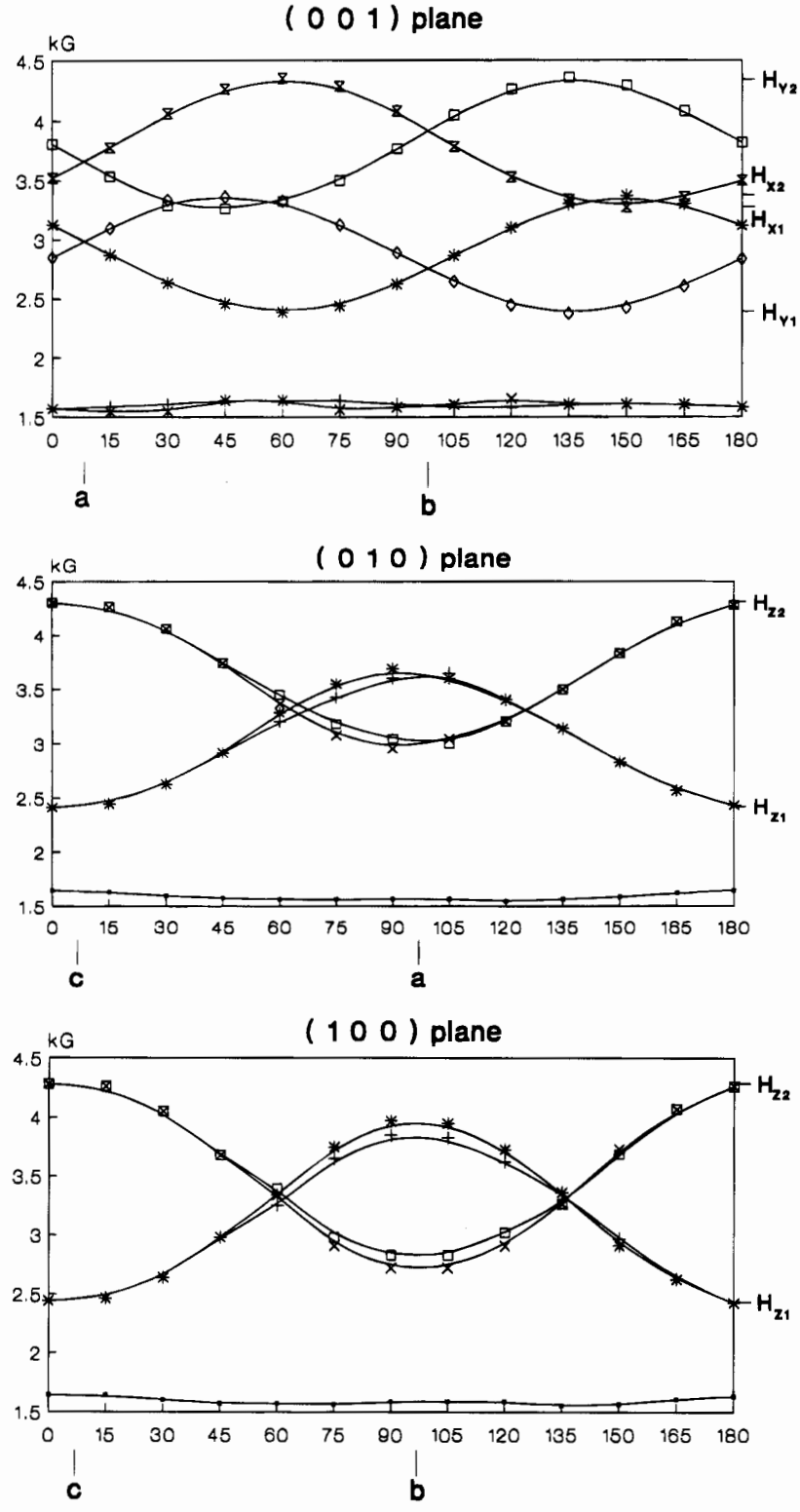

Figure 5. Angular dependence of the EPR signals (X band) of Fe(VI)-doped K_2SeO_4 (≈1.5 mol %) at 140 K (high-temperature phase) in three mutually perpendicular planes. (The displacements of the *a*, *b*, and *c* axes from 0 and 180°, as well as the presence of two sites at certain angles in the (010) and (100) planes, is caused by small crystal misalignments of about 7°).

from the regular tetrahedral symmetry, they do this in a different manner, as is outlined below. The differences between the three sites become smaller with increasing temperature, and only one position is observed above the transition to the H phase. The data collected in Table 3 further show that the symmetry splittings of the mentioned $^1E \rightarrow {}^3A_2$ transitions increase with decreasing temperature, indicating a more pronounced distortion—as was similarly deduced from the *D* values (Figure 9, Table 2).

In order to assign the three positions observed in EPR and luminescence spectroscopy to the three crystallographically independent sites in the low-temperature phase we have performed calculations within the angular overlap model,[19] the results of which are collected in Table 4. Using published ligand-field parameters,[1] $e_\sigma = 7e_\pi$ and an effective LS coupling parameter $\zeta = 130\ cm^{-1}$ within the ground state e^2 configuration, the calculated *D* values reproduce the experimental ones reasonably well—without allowing one to definitely assign the

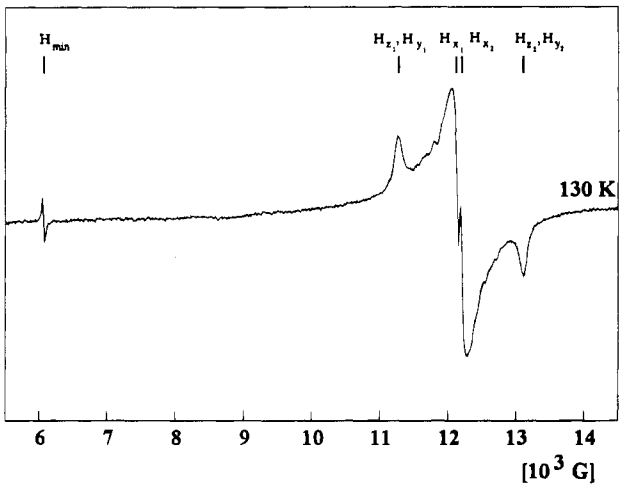

Figure 6. Powder spectrum (Q band) of Fe(VI)-doped K_2SeO_4 at 140 K (The assignment and the calculated fields are based on the parameters $D = 0.08_8$ cm^{-1}, $E = 0.02_8$ cm^{-1}, and $g = 1.99_6$).

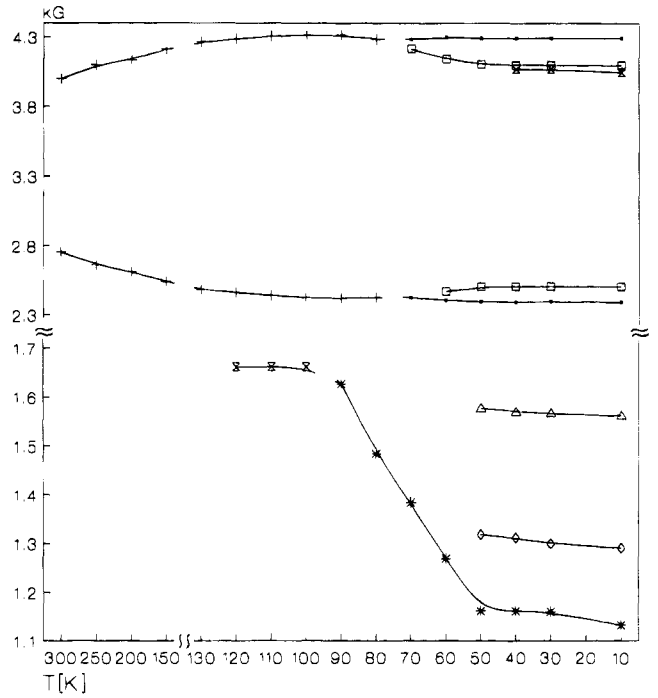

Figure 7. Temperature dependence of the observed EPR signals along [001]. (Single crystal X band data of Fe(VI)-doped K_2SeO_4; the upper and lower parts depict the $\Delta M_s = \pm 1$ and ± 2 transitions, respectively.)

observed values to specific crystallographic sites, however (Tables 2 and 4). Tentatively one may correlate Fe(VI) on the Se sites 1, 2, and 3 with the experimental D values (80 K) 0.14_2, 0.16_3, and 0.12_2 cm^{-1}, respectively—having in mind that for positions 1 and 2 the D/E ratio is near 3, while E is rather small for site 3. The calculated splittings $\delta E(^1E)$ are extremely sensitive to the chosen e_π energy, because the $^1E(e^2)$ state is π-antibonding (as the $^3A_2$ ground state and the second lowest excited term $^1A_1$ as well—both stemming from the same e^2 configuration). A slight decrease of the e_σ/e_π ratio will augment $\delta E(^1E)$ considerably but does not change the trend within the set of three values with one rather small splitting less than 3 cm^{-1}. We are again left with the situation that it is not possible to assign the observed splittings (Table 3) to Fe(VI) on certain Se positions. It is surprising at first sight that the calculated symmetry splittings of the ^1E state do not parallel the fine-

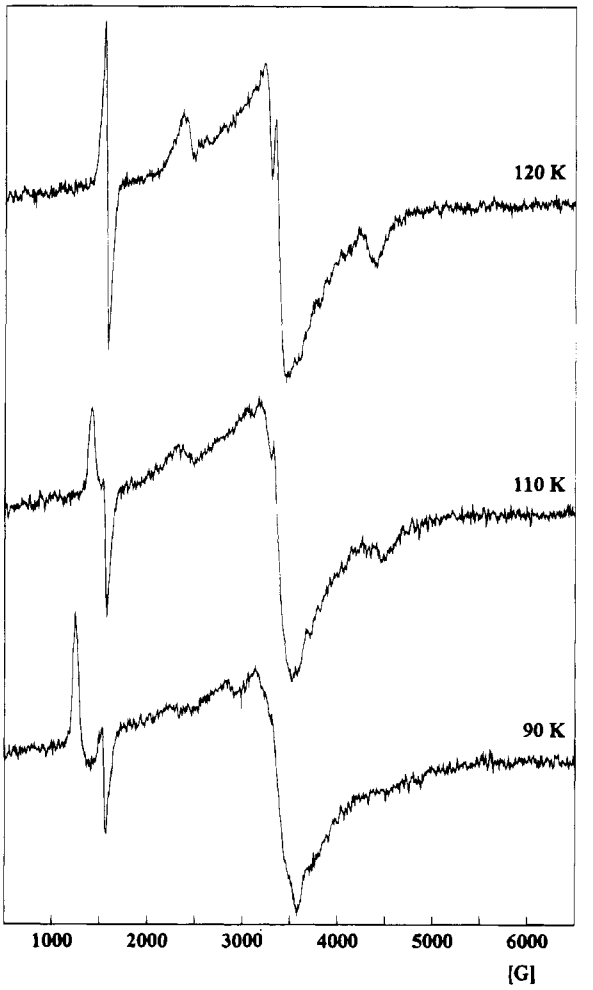

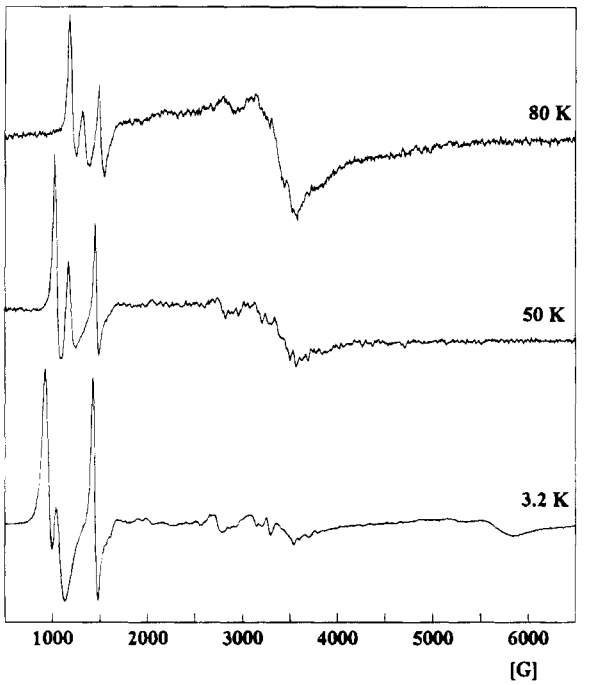

Figure 8. Temperature dependence of the powder X band EPR spectrum of Fe(VI)-doped K_2SeO_4.

structure parameters (Table 4). The reason is that the degeneracy of an orbitally 2-fold degenerate state is not lifted by trigonal ligand fields—in contrast to the situation for the $^3A_2$ ground state, which splits by any kind of lower-symmetry component. On the other hand, the calculated very small $\delta E(^1E)$ splitting of site 3 is not at all reproduced experimentally (Tables

(19) Adamsky, H.; Hoggard, P. AOMX, *a Fortran computer package*; Institut Theoret. Chemie, Heinr.-Heine-Univ. Düsseldorf, Düsseldorf, Germany.

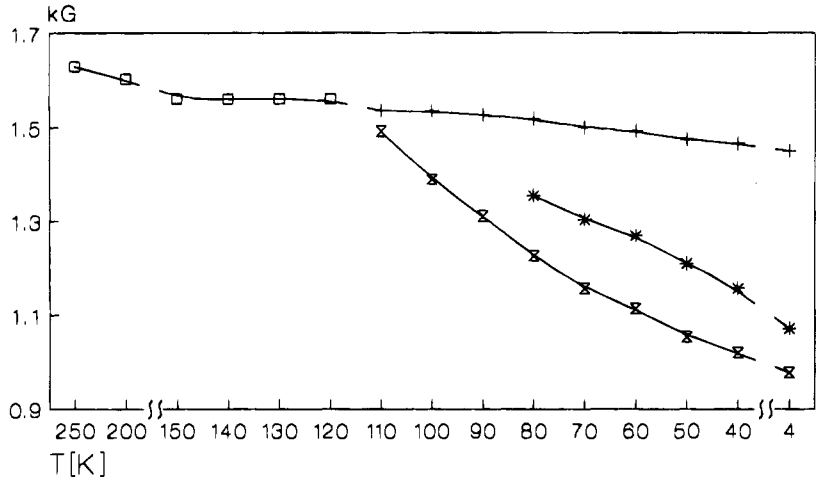

Figure 9. Temperature dependence of the H_{min} positions in the powder X band spectra of Fe(VI)-doped K_2SeO_4.

Table 2. Zero-Field Splitting Parameters D (cm^{-1}) of Fe(VI)-Doped K_2SeO_4 at Various Temperatures with the Assumptions of $D = 3E$ and, in Parentheses, $E = 0$

4 K	80 K	100 K	130 K	250 K
0.19_3 (0.22_3)	0.16_3 (0.18_8)			
0.18_3 (0.21_2)	0.14_2 (0.16_4)	0.13_5 (0.15_6)	0.09[a] (0.010)	0.06_5 (0.07_5)
0.12_3 (0.14_1)	0.10_5 (0.12_2)	0.10_0 (0.11_6)		

[a] Value from X band single crystal (Figure 5) and Q band powder spectra (Figure 6).

Table 3. Luminescence Properties (Energies in cm^{-1}) of Fe(VI)-Doped K_2SeO_4 at Various Temperatures[a]

T, K	$E(^1E)$	$\delta E(^1E)$
20[b]	6203.2	22.6
	6209.8	28.5
	6212.8	20.3
75	6204.0	20.6
	6208.7	25.7
	6211.0	19.5
120	6206	18
200	$\simeq 6203.5$	$\simeq 14.5$

[a] For definitions of $E(^1E)$, $\delta E(^1E)$, and $E(^1A_1)$, see Table 4. [b] The $E(^1A_1)$ energies (from excitation spectroscopy[2]) are 9094, 9105, and 9114 cm^{-1}, respectively.

Table 4. AOM Energies (cm^{-1})[a] of the $^3A_2$ Ground State (Split Terms at 0, $D - E$, and $D + E$) and of the Two Lowest Singlet ^1E and $^1A_1$ States for Fe(VI)-Doped K_2SeO_4 with the Parameters $e_\sigma = 7e_\pi = 12\,550$ cm^{-1} ($\Delta = 13\,000$ cm^{-1}),[b] $B = 380$ cm^{-1}, $C/B = 4.2_5$, and $\zeta = 130$ cm^{-1} [c]

		D[d]	E[d]	$E(^1E)$	$\delta E(^1E)$	$E(^1A_1)$
H		0.02_3	0.00_2	6200	0.3	11 387
L	Se(1)	0.13_4	0.03_8	6183	26.2	11 422
	Se(2)	0.17_9	0.04_9	6161	34.7	11 375
	Se(3)	0.13_5	0.02_1	6191	2.4	11 348

[a] Calculated on the basis of the SeO_4 tetrahedron geometries in the high- (295 K; H) and low-temperature (80 K; L) phases. [b] The e_σ values refers to Fe(VI) in a Se site with a Se–O spacing of $a = 1.64$ Å. e_σ (e_π) for other bond length values has been estimated by assuming an a^5 dependence. [c] D and E are the zero-field-splitting parameters, $E(^1E)$ and $\delta E(^1E)$ are the average position of the $^3A_2 \rightarrow {}^1E$ transition and the respective symmetry splitting, and $E(A_1)$ is the position of the $^3A_2 \rightarrow {}^1A_1$ transition. [d] $^3A_2$ split terms at 0.02_1, 0.02_5 cm^{-1}, at 0.09_6, 0.17_2 cm^{-1}, at 0.09_7, 0.22_8 cm^{-1}, and at 0.11_4, 0.15_5 cm^{-1}, respectively.

3 and 4), the reason most probably being an additional tetragonal vibronic Jahn–Teller component, which enhances the splitting in the case of a near-degeneracy of the ^1E components.[20] Such an effect is well-known for the first excited ^2E state in Cr^{3+}-doped Al_2O_3 for example. One should finally state that the D and E energies depend only slightly on the e_σ/e_π ratio, but strongly on the chosen ζ value—in contrast to the splitting of the ^1E term, which shows a reverse behavior. A decrease of the effective LS coupling constant induces smaller zero-field splittings but again without changing the trend with respect to the three Se positions. The reason for the failure to correlate the 80 K EPR data with the calculated values based on the structural results at 80 K [16] in a more definite way is most probably that the standard deviations of the Se–O spacings and the O–Se–O angles in the low-temperature phase amount to nearly 0.02 Å and 1°, respectively,[16] which indeed introduces a considerable tolerance range in the magnitudes of the calculated values. One may also argue that Fe(VI) not necessarily adopts the host site geometry. Considering though that the ionic radii of tetrahedral Fe^{6+} and Se^{6+} are comparable (0.25 and 0.28 Å, respectively[21]) and that electronic effects of the Jahn–Teller type (orbitally nondegenerate ground state in T_d) are absent, this argument is not convincing.

With the chosen B value and C/B ratio (Table 4) the ^1E state energy is reproduced correctly, while the $^1A_1$ term is observed at about 2300 cm^{-1} lower energy (Tables 3 and 4). Using the concept of Jorgensen,[22] who introduced different B values for different one-electron configurations (here e^2, $e^1t_2^1$, t_2^2) in the case of more covalent transition metal compounds, one would have rather expected that ligand field theory works sufficiently well with a single B_{ee} parameter, because the involved terms $^3A_2$, ^1E, and $^1A_1$ originate from the same e^2 configuration. However, the strong covalency of the Fe(VI)–O bond, as documented by the low-lying charge-transfer band around 19 000 cm^{-1},[2] has led to an intermixing of a e^3L charge-transfer contribution (L: ligand hole) into the $^1A_1$ state with a corresponding energy lowering due to a more strongly reduced B value. This phenomenon is studied in greater detail by Atanasov elsewhere.[23] In agreement with this consideration are the optical results for tetraoxo-coordinated Mn(V) and Cr(IV). While in the latter case[4] ligand field theory in the modified form according to Jorgensen can be applied—the Cr(IV)–O bond is much less covalent and the lowest-energy charge transfer transition appears in the UV region—the case of Mn(V)[6] is intermediate between Fe(VI) and Cr(IV).

The above arguments may qualitatively explain as well why the effective LS coupling constant deduced from the g-value (eq 1) is as low as 20 cm^{-1}, while the one used to reproduce the $^3A_2$ ground state zero-field splitting (Table 4) is much higher.

(20) Oetliker, U.; Herren, M.; Güdel, H. U.; Kesper, U.; Albrecht, C.; Reinen, D. *J. Chem. Phys.* **1994**, *100*, 8656.
(21) Shannon, R. D. *Acta Crystallogr.* **1976**, *A32*, 751.
(22) Schäffer, C. E.; Jorgensen, C. K. *J. Inorg. Nucl. Chem.* **1962**, *4*, 73.
(23) Atanasov, M. To be published.

While in the former case the orbital contributions reflect interactions mainly with the excited triplet state $^3T_2(e^1t_2^1)$ at 13 000 cm^{-1} near the charge-transfer band around 19 000 cm^{-1}, *LS* coupling effects involving the low-lying e^2 terms ^1E and $^1A_1$ might be of dominating influence on the zero-field splitting. This point needs further clarification, however.

The deduced e_σ/e_π ratio (Table 4) is unusually large for a π-donor such as oxygen. Whether this result represents a true physical effect or if it is due to the partial breakdown of ligand field theory remains unanswered at present.

Summary

1. The single crystal and powder EPR spectra of Fe(VI)-doped K_2CrO_4, β-K_2SO_4, and K_2SeO_4 (high-temperature phase of space group *Pnam*) allow one to determine the orientations of the fine structure components and their magnitudes. While D_z is oriented parallel to the crystallographic *c* direction and perpendicular to the molecular C_s plane of the FeO_4 tetrahedra, D_y and D_x lie in the (001) plane—with D_y near the *a* direction for $D \gg E$ and strongly rotated toward the *b* axis for *D* approaching 3*E*.

2. The zero-field splitting parameters of Fe(VI) derived from the EPR powder spectra could be used as a probe for the geometrical changes of the SeO_4 host tetrahedra in K_2SeO_4 when passing the phase transitions at 130 and 93 K. In the low-temperature phase (space group $Pna2_1$) with a tripled *a* axis three differently distorted sites are observed. The extent of deformation diminshes with increasing temperature, leading to two (nearly) collapsing positions in the incommensurate phase existing in the intermediate temperature region (space group *Pnam*, structure modulation along *a*). Above about 120 K only one crystallographically independent position is left.

3. AOM calculations for Fe(VI) in the L phase on the basis of the published geometries of the three SeO_4 host polyhedra with a reasonable parameter set yielded fine structure parameters and energy splittings of the first excited ^1E state in rough correspondence with the experimental values from EPR and luminescence spectroscopy. It was not possible, however, to assign the observed spectroscopic features to a specific crystallographic site unambigously.

4. The EPR study confirms the results from optical and luminescence spectroscopy that Fe(VI) isomorphically substitutes the tetrahedrally coordinated Cr(VI), S(VI), and Se(VI) cations in host compounds K_2MO_4—similar to the also d^2 configurated Mn(V)[5,20] and Cr(IV) centers,[4] which substitute P(V), V(V) and Ge(IV), Si(IV), respectively, in various oxidic solids.

Acknowledgment. The authors owe thanks to Dr. G.-G. Lindner (Marburg, Germany) for having performed the AOM calculations. Financial support by the Deutsche Forschungsgemeinschaft and the Swiss National Science Foundation is gratefully acknowledged.

IC940954O